Modeling of a three-axes MEMS gyroscope with feedforward PI quadrature compensation

D. Marano[1], A. Cammarata[2*], G. Fichera[2], R. Sinatra[2], D. Prati[3]

[1] Department of Engineering ”Enzo Ferrari”, University of Modena and Reggio Emilia, Italy. E-mail: acamma@diim.unict.it

[2] Dipartimento Ingegneria Civile e Architettura, University of Catania, Italy. E-mail: acamma@diim.unict.it, gabriele.fichera@dii.unict.it, rsinatra@dii.unict.it

[3] ST Microelectronics, Catania, Italy, E-mail: daniele.prati@st.com

[*]Corresponding author. Tel.: +39-095-738-2403 ; fax: +39 0931469642. E-mail address: acamma@diim.unict.it

Abstract: The present paper is focused on the theoretical and experimental analysis of a three-axes MEMS gyroscope, developed by ST Microelectronics, implementing an innovative feedforward PI quadrature compensation architecture. The gyroscopes structure is explained and equations of motion are written; modal shapes and frequencies are obtained by finite element simulations. Electrostatic quadrature compensation strategy is explained focusing on the design of quadrature cancellation electrodes. A new quadrature compensation strategy based on feedforward PI architecture is introduced in this device to take into account variations of device parameters during lifetime. Obtained results show a significant reduction of the quadrature error resulting in a improved performance of the device. Fabrication and test results conclude the work.

Keywords: Quadrature error, MEMS, Gyroscope, FEM modeling, Electrostatic quadrature compensation, Feedforward PI.

1 Introduction

Gyroscopes are physical sensors that detect and measure the angular rotations of an object relative to an inertial reference frame. MEMS gyroscopes are typically employed for motion detection (e.g. in consumer electronics and automotive control systems), motion stabilization and control (e.g. antenna stabilization systems, 3-axis gimbals for UAV cameras) [1]. Combining MEMS gyroscopes, accelerometers and magnetometers on all three axes yields an inertial measurement unit (IMU); the addition of an on-board processing system computing attitude and heading leads to a AHRS (attitude and heading reference system), highly reliable device, in common use in commercial and business aircrafts. Measurement of the angular position

© Springer International Publishing AG 2017

B. Eynard et al. (eds.), *Advances on Mechanics, Design Engineering and Manufacturing*, Lecture Notes in Mechanical Engineering,
DOI 10.1007/978-3-319-45781-9_8

in rate gyroscopes can be achieved by numerical integration of the gyroscope's output; the time integration of the output signal, together with the associated errors and noise, leads to orientation angle drifts [2]-[4]. Among all the major error sources, the undesired sense-mode vibration resulting from the coupling of drive-mode displacement and sense mode of the gyroscope is the mechanical quadrature signal [5]-[11]. Since its magnitude can reach thousand degrees per second, the measurement of a low electric signal generated by very small Coriolis force in presence of a much bigger electric signal becomes a difficult problem [12]. Several techniques, based either on mechanical or electronic principles, have been proposed for quadrature error compensation; among all, an efficient approach able to provide a complete quadrature error cancellation is the electrostatic quadrature compensation. This approach is based on the electromechanical interaction between properly designed mechanical electrodes and the moving mass of the gyroscope: electrostatic forces, mechanically balancing quadrature forces, are generated biasing electrodes with differential dc voltages [13]-[18]. In most devices, the magnitude of biasing dc voltages is determined in order to nullify an experimentally measured quadrature error. In this way, however, it is not possible changing the dc voltages during the lifetime of the device to accomplish variations of structural device properties. A possible solution to this problem is addressed in the present paper, where an innovative feed-forward PI quadrature compensation architecture implemented on a novel three-axes MEMS gyroscope, manufactured by ST Microelectronics, is discussed.

2 Gyroscope Structure And Dynamics

2.1 Structure

The three-axes Coriolis Vibrating Gyroscope presented in the following is a compact device, manufactured by ST Microelectronics, combining a triple tuning-fork structure with a single vibrating element. The device is fabricated using *ThELMA-ISOX (Thick Epipoly Layer for Microactuators and Accelerometers)* technology platform, a surface micromachining process proprietary of ST Microelectronics. This platform allows to obtain suspended seismic masses electrically isolated but mechanically coupled with high and controlled vacuum inside the cavity of the device. The structure (Fig.1) is composed of four suspended plates ($M_{1,2,3,4}$) coupled by four folded springs, elastically connected to a central anchor by coupling springs. The fundamental vibration mode (driving mode) consists of a planar oscillatory radial motion of the plates: globally, the structure periodically expands and contracts, similarly to a "beating heart". Plates $M_{1,2}$ are actuated by a set of comb-finger electrodes and the motion is transmitted to the secondary plates $M_{3,4}$ by the folded springs at the corners. The sensing modes of the device consist of two out-of-plane modes (Roll and Pitch) characterized by counter-phase oscillation of plates $M_{1,2}$ ($M_{3,4}$) and one in-plane counter-phase motion of the yaw plates ($M_{3,4}$) (Yaw mode). Rotation of

yaw plates ($M_{3,4}$) is measured by a set of parallel-plate electrodes, $PP_{1,2}$, located on the yaw plates. Pitch and roll angular rotations are measured sensing the capacitive variations between each plate and an electrode placed below (respectively $R_{1,2}$ and $P_{1,2}$ for roll and pitch masses); the driving mode vibration is measured by additional comb-finger electrodes $SD_{1,2}$. Electrostatic quadrature compensation is implemented on Roll (Quadrature Compensation Roll, QCR) and Pitch axis (QCP) by means of electrodes placed under each moving mass. Yaw axis quadrature compensation electrodes (QCY) are slightly different from the ones of other axis since they are not placed underneath the moving mass and have height equal to the gyroscope's rotor mass.

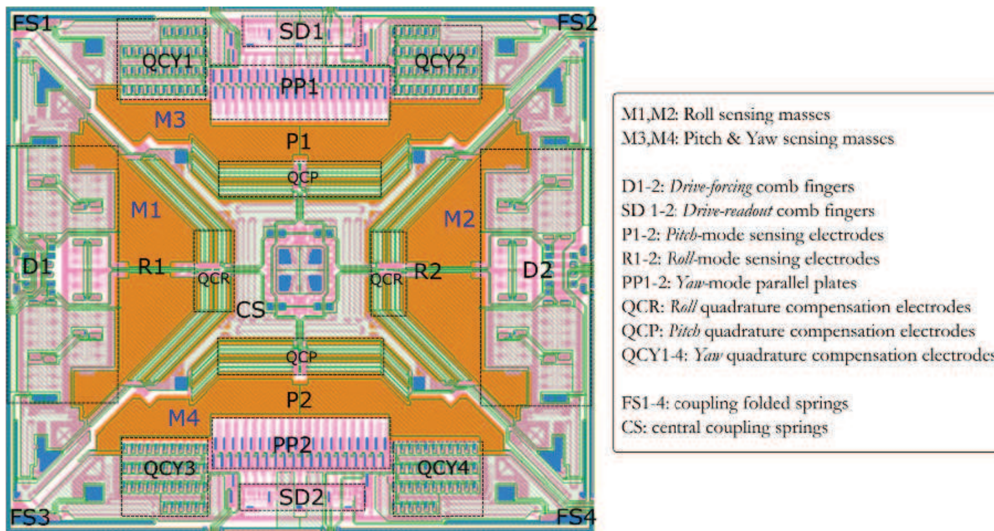

Fig. 1: Case-study gyroscope layout

2.2 Dynamics

The gyroscope's equations of motion are derived in the general case in [4, 19]. The coordinate-system model shown in Fig. 2 consists of three coordinate frames respectively defined by their unit vectors $\Sigma_i = [X, Y, Z]$; $\Sigma_p = [x, y, z]$; $\Sigma = [\hat{x}, \hat{y}, \hat{z}]$. The frame Σ_i represents the inertial reference system, Σ_p is the inertial platform frame, Σ is a body-frame with origin at a point P of a moving body (for a 3-axes gyroscope the considered body is one of the four moving suspended plates and the platform frame is usually assigned to the fixed silicon substrate). For a decoupled three axes gyroscope simplifying assumptions (constant angular rate inputs, operating frequency of the gyroscope much higher than angular rate frequencies) can be done [19, 20], and the equations of motion (EoM) become:

$$m\ddot{r}_x + c_x\dot{r}_x + k_x r_x = -2m\Omega_y\dot{r}_z + 2m\Omega_z\dot{r}_y + F_{D_x} \tag{1a}$$
$$m\ddot{r}_y + c_y\dot{r}_y + k_y r_y = 2m\Omega_x\dot{r}_z - 2m\Omega_z\dot{r}_x + F_{D_y} \tag{1b}$$
$$m\ddot{r}_z + c_z\dot{r}_z + k_z r_z = -2m\Omega_x\dot{r}_y + 2m\Omega_y\dot{r}_x + F_{D_z} \tag{1c}$$

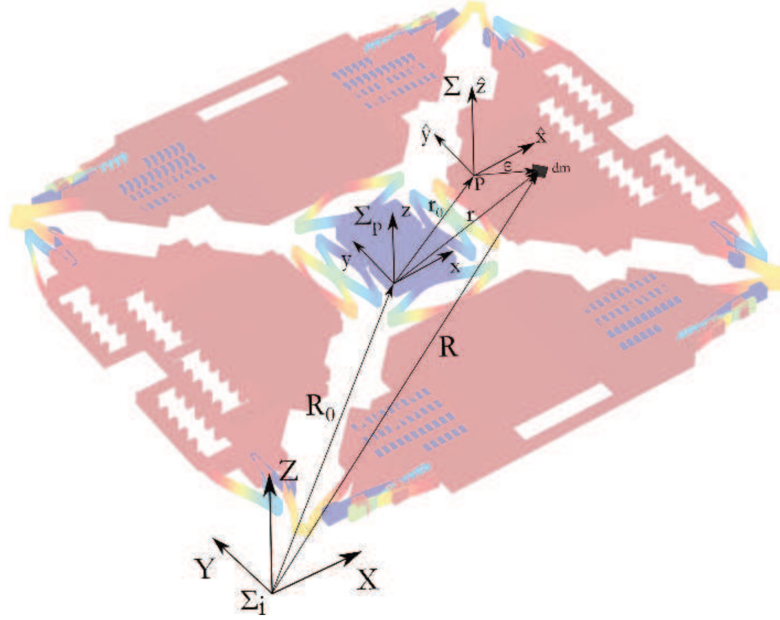

Fig. 2: Coordinate system model for the derivation of kinematic equations

2.2.1 Modal analysis

The device eigenfrequencies are determined by FEM simulation (Fig. 3). As imposed by mechanical design the fundamental mode of vibration consists of an in-plane inward/outward radial motion of the plates in which the structure cyclically expands and contracts. Several spurious modes at higher frequencies, not reported here for brevity, have been also identified.

3 Electrostatic quadrature cancellation

3.1 Quadrature force

The dynamics equations of a linear yaw vibrating gyroscope can be expressed, considering the off-diagonal entries of the mechanical stiffness matrix, as

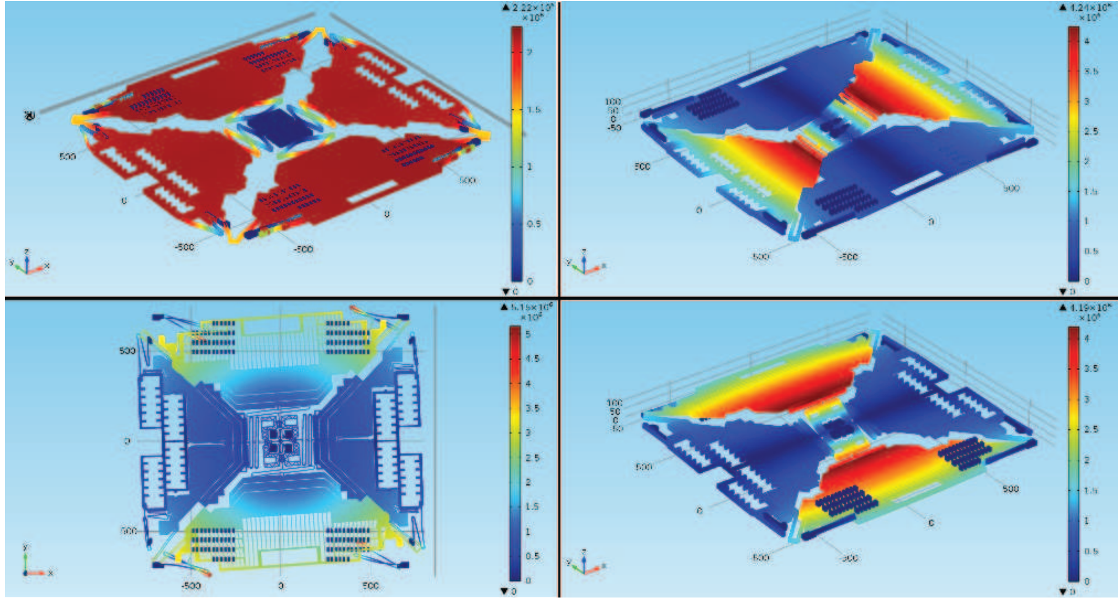

Fig. 3: Fundamental vibration modes (drive, pitch, yaw, roll)

$$\begin{bmatrix} m & 0 \\ 0 & m \end{bmatrix} \ddot{\mathbf{p}}(t) + \begin{bmatrix} d_x & 0 \\ 0 & d_y \end{bmatrix} \dot{\mathbf{p}}(t) + \begin{bmatrix} k_x & k_{xy} \\ k_{yx} & k_y \end{bmatrix} \mathbf{p}(t) = \begin{bmatrix} F_d \\ F_C \end{bmatrix} \tag{2}$$

where $\mathbf{p}(t) = [x(t), y(t)]^T$ is the position vector of the mass in drive and sense direction, m represents the Coriolis mass, d_x (d_y) and k_x (k_y) represent the damping and stiffness along the X-axis (Y-axis); k_{xy} (k_{yx}) are the cross coupling stiffness terms bringing the quadrature vibration response; F_d is the driving force and F_C is the Coriolis force. The dynamic equation in sense direction can be expressed as

$$m\ddot{y} + d_y\dot{y} + k_y y = F_C + F_q \tag{3}$$

where $F_C = -2m\Omega_z\dot{x}$ is the Coriolis force and $F_q = -k_{yx}x$ is the quadrature force. *The Coriolis mass is usually actuated into resonant vibration with constant amplitude in drive direction*, thus the drive-mode position can be expressed by $x(t) = A_x \sin(\omega_x t)$. Introducing the sinusoidal drive movement, Coriolis and quadrature force can be expressed as

$$F_C = 2m\Omega_z\omega_x A_x \cos(\omega_x t), \quad F_q = -k_{yx}A_x sin(\omega_x t) \tag{4}$$

3.2 Quadrature cancellation electrodes design

Quadrature compensation electrodes for out-of-plane Roll (Pitch) motion are shown in Fig. 4; the electrostatic force generated by the *i*-th electrode is given by

$$F_{R,P_i} = \pm\frac{1}{2}\epsilon_0 \frac{\left(\frac{H_0}{2} \pm A_x \sin(\omega_x t)\right) L_0}{(g)^2} (V \pm \Delta V)^2 \tag{5}$$

where $A_x \sin(\omega_x t) = x(t)$ is the drive movement, H_0 and L_0 are respectively width and length of quadrature compensation electrodes and g is the air gap. The voltage sign is chosen either positive $(V + \Delta V)$ or negative $(V - \Delta V)$ according to the electrode biasing, whereas the x sign is chosen according to the overlap variation among the proof mass and quadrature compensation electrodes (QCE) as shown in Fig. 4. The total force is obtained as the product of the force generated by a single electrode by the number n of electrodes: $F_{tot} = \sum_i F_i \cdot n$.

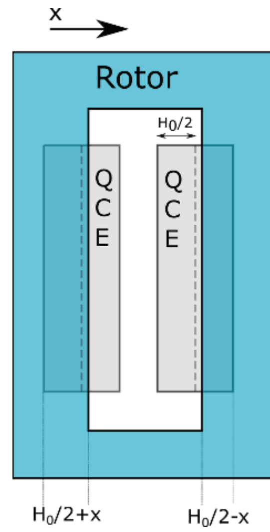

Fig. 4: Roll (Pitch) quadrature compensation electrode; detail of Fig. 1 (QCR and QCP electrodes)

The quadrature force F_Q (Eq. (4)) is balanced by the drive dependent component of the electrostatic force, properly tuning the ΔV potential applied to the pitch (roll) quadrature compensation electrodes:

$$k_{yx} A_x sin(\omega_x t) = \frac{1}{2}\epsilon_0 \frac{A_x \sin(\omega_x t) L_0}{(g)^2} (V \pm \Delta V)^2 \tag{6}$$

Quadrature compensation electrodes for the in-plane yaw motion are shown in Fig. 5. The electrostatic force generated by the *i*-th electrode is given by

$$F_{Y_i} = \pm\frac{1}{2}\epsilon_0 h \frac{(L_{OV} \pm x)}{(g \pm y)^2} (V \pm \Delta V)^2 \tag{7}$$

where h denotes the electrodes height and g the air gap between the moving mass and the quadrature compensation electrode.

Design parameters of quadrature cancellation electrodes for the three-axes gyro are reported in Tab. 1 respectively for roll (pitch) and yaw electrodes. Quadrature compensation forces are regulated tuning the differential voltage ΔV such that the

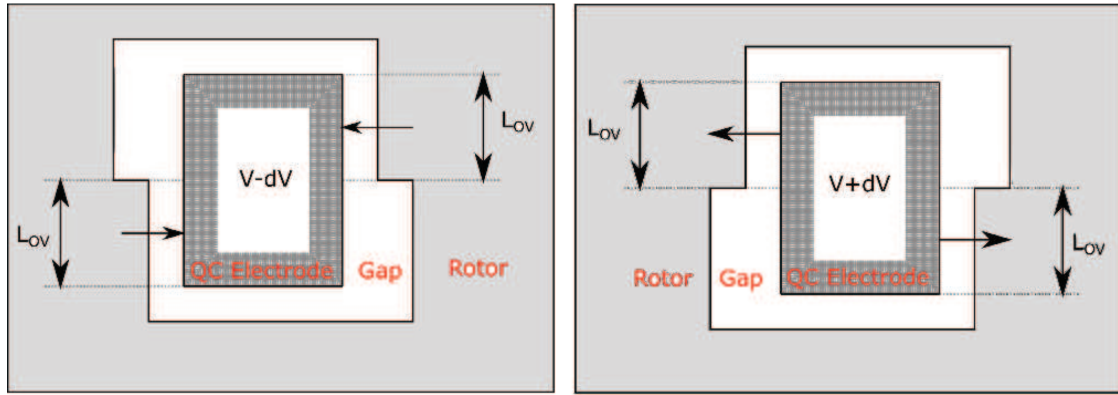

Fig. 5: Yaw quadrature compensation electrode; detail of $QCY_{2,3}$ electrodes in Fig. 1

Table 1: Quadrature compensation electrodes parameters

Axis	g $[\mu m]$	H_0 $[\mu m]$	L_0 $[\mu m]$	L_{OV} $[\mu m]$	h $[\mu m]$
Roll (Pitch)	1.2	20	1200	-	-
Yaw	1.1	-	-	25	24

residual quadrature is canceled out; the ΔV value corresponding to the minimum residual quadrature is denoted by ΔV_{Opt}. Residual quadrature signals are reported in Tab. 2

3.3 Feedforward PI architecture

Quadrature is measured for each device during the electric wafer sorting test, here tension variation ΔV_{opt} is set for each device during the calibration phase. A serious limit of this approach is that structural parameters of devices can change unpredictably during lifetime, causing variations of quadrature error. The value of ΔV_{Opt} is therefore no longer an optimal value for the new operating conditions. A proposed solution to this problem is to adopt a closed loop architecture, based on feedforward PI in which the optimal ΔV_{Opt} is the feedforward action and PI controller compensates for lifetime quadrature variations. This procedure results in a further optimization of residual quadrature values, as shown in Tab. 2.

Table 2: Residual quadrature results

Axis	Residual quadrature OL [Nm]	Residual quadrature CL [Nm]
Pitch	$6.46 \cdot 10^{-12}$	$2.04 \cdot 10^{-16}$
Roll	$9.09 \cdot 10^{-12}$	$2.87 \cdot 10^{-16}$
Yaw	$3.66 \cdot 10^{-13}$	$1.15 \cdot 10^{-17}$

4 Fabrication and test results

All individual devices present on the wafer are tested for functional defects by electric wafer sorting (EWS). The quadrature amplitude is evaluated for each gyroscope of the wafer, as shown in Fig. 6.

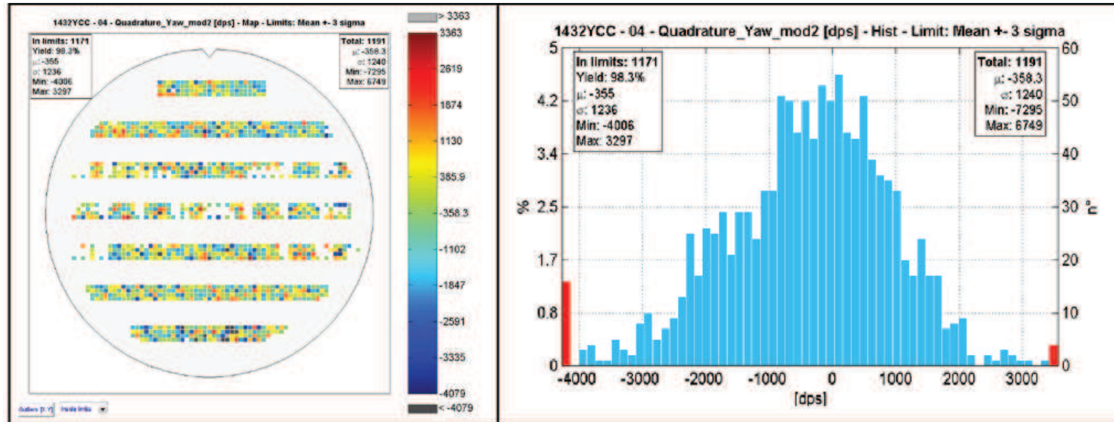

Fig. 6: EWS Testing: quadrature distribution (Yaw axis) on wafer

4.1 *Experimental quadrature cancellation*

The quadrature compensation strategy has been electrically simulated for an isolated device inside the wafer. Applying a differential dc voltage to quadrature compensation electrodes quadrature error variation is observed and ΔV_{Opt} value is obtained by interpolation; in Fig. 7 results for roll axis are shown.

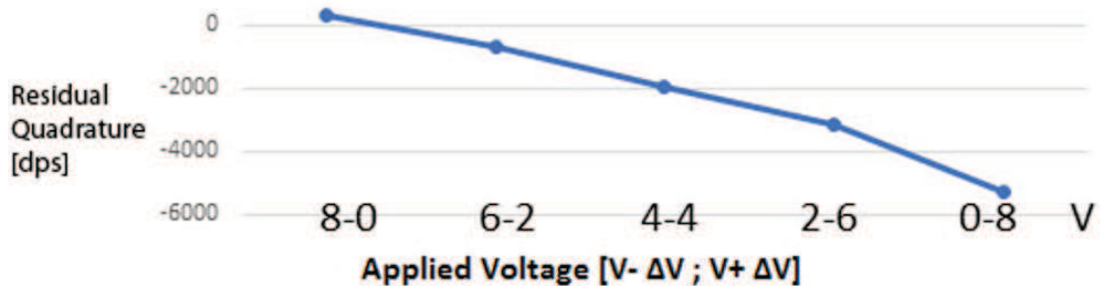

Fig. 7: Residual quadrature amplitude (Roll axis) for different voltages applied to Roll quadrature cancellation electrodes

5 Conclusion

In this paper a theoretical and experimental analysis of a three-axes MEMS gyroscope, developed by ST Microelectronics, has been presented. Exploiting the equations of motions for a 3-DoF gyroscope structure provided an estimation of the drive and sense motion amplitude. Natural mode shapes and frequencies of the device have been obtained by finite element simulations to characterize the device. Equations for the design of quadrature compensation electrodes have been derived, and residual quadrature calculated with open loop architecture. A new quadrature compensation strategy, based onan innovative feedforward PI architecture, accomplishing for changes of device parameters during lifetime of device has been introduced and results discussed. Finally, fabrication details and measurement results of test devices have been reported.

References

1. V. Kaajakari, Practical MEMS, Small gear publishing, Las Vegas, Nevada, 2009
2. M. Saukoski, L. Aaltonen, K.A.I. Halonen, Zero-Rate Output and Quadrature Compensation in Vibratory MEMS Gyroscopes", IEEE Sensors Journal, Vol.7, No. 12, December 2007
3. B.R. Johnson, E. Cabuz, H.B. French, and R. Supino, Development of a MEMS gyroscope for northfinding applications, in Proc. PLANS, Indian Wells, CA, May 2010, pp. 168-170.
4. Volker Kempe, Inertial MEMS, Principles and Practice, Cambridge University Press, 2011
5. A. S. Phani, A. A. Seshia, M. Palaniapan, R. T. Howe, and J. A. Yasaitis, Modal coupling in micromechanical vibratory rate gyroscopes, IEEE Sensors J., vol. 6, no. 5, pp. 11441152, Oct. 2006.
6. H. Xie and G. K. Fedder, Integrated microelectromechanical gyroscopes, J. Aerosp. Eng., vol. 16, no. 2, pp. 6575, Apr. 2003.
7. W. A. Clark, R. T. Howe, and R. Horowitz, Surface micromachined Z-axis vibratory rate gyroscope, in Tech. Dig. Solid-State Sensor and Actuator Workshop, Hilton Head Island, SC, USA, Jun. 1996, pp. 283287.
8. A. Cammarata, and G. Petrone, Coupled fluid-dynamical and structural analysis of a monoaxial mems accelerometer, The International Journal of Multiphysics 7.2 (2013): 115-124.
9. S. Pirrotta, R. Sinatra, and A. Meschini, A novel simulation model for ring type ultrasonic motor, Meccanica 42.2 (2007): 127-139.
10. M. S. Weinberg and A. Kourepenis, Error sources in in-plane silicon tuning fork MEMS gyroscopes, J. Microelectromech. Syst., vol. 15, no. 3, pp. 479491, Jun. 2006.
11. Mikko Saukoski, System and circuit design for a capacitive MEMS gyroscope, Doctoral Dissertation, Helsinki University of Technology
12. R. Antonello, R. Oboe, L. Prandi, C. Caminada, and F. Biganzoli, Open loop compensation of the quadrature error in MEMS vibrating gyroscopes, IEEE Sens. J., vol. 7, no. 12, pp. 1639-1652, Dec. 2007
13. Ni, Yunfang, Hongsheng Li, and Libin Huang. "Design and application of quadrature compensation patterns in bulk silicon micro-gyroscopes." Sensors 14.11 (2014): 20419-20438.
14. W. A. Clark and R. T. Howe, Surface micromachined z-axis vibratory rate gyroscope, in Proc. Solid-State Sens., Actuators, Microsyst. Work-shop, Hilton Head Island, SC, Jun. 1996, pp. 283-287
15. E. Tatar, S. E. Alper and T. Akin, Quadrature error compensation and corresponding effects on the performance of Fully decoupled MEMS gyroscopes, IEEE J. of Microelectromechanical systems, vol. 21, no. 3, June 2012

16. A. Sharma, M.F. Zaman, and F. Ayazi, A sub $0.2°/hr$ bias drift micromechanical gyroscope with automatic CMOS mode-matching, IEEE J. of Solid-State Circuits, vol. 44, no. 5, pp. 1593-1608, May 2009
17. B. Chaumet, B. Leverrier, C. Rougeot, and S. Bouyat, A new silicon tuning fork gyroscope for aerospace applications, in Proc. Symp. Gyro Technol., Karlsruhe, Germany, Sep. 2009, pp. 1.1-1.13
18. Weinberg, M.S., Kourepenis A., Error sources in in-plane silicon tuning-fork MEMS gyroscopes, *Journal of Microelectromechanical Systems*. Volume 15, Issue 3, June 2006, pp. 479-491
19. C. Acar, A. Shkel, MEMS Vibratory Gyroscopes, Structural Approaches to Improve Robustness, Springer, 2008.
20. Acar, C., Shkel, A. M. (2003). Nonresonant micromachined gyroscopes with structural mode-decoupling. Sensors Journal, IEEE, 3(4), 497-506.